PHOTONICS Research

Dynamic performance and reflection sensitivity of quantum dot distributed feedback lasers with large optical mismatch

Bozhang Dong,[1,*] Jianan Duan,[1,7] Heming Huang,[1] Justin C. Norman,[2,3] Kenichi Nishi,[4] Keizo Takemasa,[4] Mitsuru Sugawara,[4] John E. Bowers,[2,3,5] and Frédéric Grillot[1,6]

[1]LTCI, Télécom Paris, Institut Polytechnique de Paris, 19 Place Marguerite Perey, 91120 Palaiseau, France
[2]Institute for Energy Efficiency, University of California, Santa Barbara, California 93106, USA
[3]Materials Department, University of California, Santa Barbara, California 93106, USA
[4]QD Laser, Inc., Kawasaki, Kanagawa 210-0855, Japan
[5]Department of Electrical and Computer Engineering, University of California, Santa Barbara, California 93106, USA
[6]Center for High Technology Materials, University of New-Mexico, Albuquerque, New Mexico 87106, USA
[7]Current address: State Key Laboratory on Tunable Laser Technology, School of Electronic and Information Engineering, Harbin Institute of Technology, Shenzhen 518055, China
*Corresponding author: bozhang.dong@telecom-paris.fr

Received 1 February 2021; revised 26 May 2021; accepted 22 June 2021; posted 22 June 2021 (Doc. ID 421285); published 29 July 2021

This work reports on a high-efficiency InAs/GaAs distributed feedback quantum dot laser. The large optical wavelength detuning at room temperature between the lasing peak and the gain peak causes the static, dynamic, and nonlinear intrinsic properties to all improve with temperature, including the lasing efficiency, the modulation dynamics, the linewidth enhancement factor, and consequently the reflection insensitivity. Results reported show an optimum operating temperature at 75°C, highlighting the potential of the large optical mismatch assisted single-frequency laser for the development of uncooled and isolator-free high-speed photonic integrated circuits.

https://doi.org/10.1364/PRJ.421285

1. INTRODUCTION

In recent years, progress in monolithic photonic integration technologies has paved the way for future low-cost, energy-efficient, large-scale, and small-footprint photonic integrated circuits (PICs) [1]. High performance on-chip light sources with single-frequency behavior, especially distributed feedback (DFB) semiconductor lasers play a crucial role in versatile applications, including high-resolution LIDAR systems [2], high-speed supercomputers, and optical data centers [3]. Owing to their narrow linewidth and large modulation bandwidth [4,5], DFB lasers that are spatially and spectrally single mode are useful for wavelength-division multiplexing (WDM) and can support the large growing data transmission rate in this Big Data era. In DFBs, the optical wavelength detuning (OWD), that is to say, the wavelength mismatch between the DFB lasing wavelength and the gain peak, plays a huge role in the device performance. In particular, a strong operation stability is required over a wide temperature range in silicon-based integrated technologies. Nevertheless, prior studies revealed that a positive OWD leads to a degradation of the laser physical characteristics such as the threshold current and the resonance frequency, hence limiting their use for high-speed transmission when the temperature is out of the optimum condition [6,7]. On the other hand, another major challenge is the development of isolator-free PICs. To this end, the laser sensitivity to parasitic reflections, which directly result from the various active and passive transitions and regrowth interfaces, is of paramount importance to be taken into account [8]. Prior studies on the external optical feedback (EOF) dynamics of semiconductor lasers revealed that those unwanted reflections lead to strong laser destabilization, such as mode-hopping, low-frequency fluctuations, and coherence collapse [9–11], whose presence degrades the power penalty and transmission performance of lasers [12,13]. To overcome these issues, on-chip optical isolators have been considered, however, at the price of poor isolation performance, high cost, and large footprint for a PIC [14]. To develop high-efficiency, single-frequency light sources for isolator-free applications, a quantum confined active region made with self-assembled quantum dots (QDs) is a promising solution. With the charge carrier confinement in the three spatial dimensions, the energy levels are completely discrete in those nanostructures with zero dimensionality. Prior studies demonstrated that semiconductor lasers made with these nanocrystals lead to high lasing efficiency [15,16], low relative

intensity noise [17–19], remarkable temperature stability [20], and high tolerance for EOF [21–23]. More recently, it has been shown that epitaxial QD lasers directly grown on silicon are interesting for integrated technologies since they are less sensitive to the dislocations arising during the epitaxial growth of III-V groups on silicon compared to their quantum well (QW) counterparts [24]. In this context, the high thermal stability of QDs together with the large optical mismatch can be considered to realize efficient quantum light emitters customized for high-temperature operation. In this work, we report on an efficient 1.3 μm InAs QD DFB laser on GaAs that has a large OWD at room temperature. By controlling the OWD with temperature, namely, the shift of the gain peak with respect to the DFB oscillation wavelength [25], we analyze its light emission characteristics from 15°C to 55°C. In particular, we link the influence of this optical detuning to the static, dynamic, and nonlinear characteristics of the QD laser. With the design of an optimum condition at 75°C, results reported demonstrate that all the performance characteristics of the DFB laser are improved with temperature. For instance, the multimode lasing emission that takes place across the gain peak and due to temperature-dependent homogeneous linewidth broadening mechanisms associated with different QD populations [26,27] is completely eliminated; moreover, the threshold current, the linewidth enhancement factor (α factor), the noise properties, the modulation dynamics, and the reflection insensitivity are all greatly improved. In particular, the laser demonstrates a very strong robustness against EOF at a high temperature of 55°C, in the absence of any unstable behavior with a strong feedback strength of 25% (−6 dB). This study aims at giving a guideline for designing high-performance single-frequency lasers that can be applied to an isolator-free and uncooled integrated system.

The paper is organized as follows. Section 2 introduces the QD DFB laser and its static characteristics. In Section 3, the noise properties and dynamics of the device studied are analyzed. In Section 4, we perform the measurements of the linewidth enhancement factor of laser. Then, a detailed analysis of the laser dynamics in optical feedback operation is presented in Section 5. In Section 6, we conclude our results.

2. DESCRIPTION OF THE QD DEVICE

The active region of the device under study is grown from eight-layer InAs QDs on (100) GaAs substrate by using molecular beam epitaxy. The density of QDs is $\sim 6 \times 10^{10}$ cm^{-2} per layer. Each dot layer was separated by a p-doped GaAs spacer, which is beneficial for further increasing the modal gain up to about 50 to 60 cm^{-1}. The luminescence width at half-maximum of the active region is as narrow as ∼24 meV at room temperature, which means the inhomogeneous broadening caused by the size and shape distribution of the QDs is quite low. Uniform QDs are highly beneficial for improving laser performance, including the increase of thermal stability [20,28], the reduction of α factor [20], the improvement of insensitivity to backreflections, and ensuring a single-mode emission with low threshold and high efficiency [28].

The corrugated structure above the active region is fabricated with electron beam lithography and wet etching, and the InGaP/GaAs gratings on top are formed by metal organic vapor phase epitaxy. The cavity length L_{cav} and the coupling coefficient κ are designed to be 750 μm and 16 cm^{-1}, respectively, and thus a normalized coupling coefficient κL of 1.2 is applied to avoid strong longitudinal spatial hole burning (LSHB) [27,29]. The laser is designed to operate at a high temperature, and thus the OWD between the gain peak and the DFB oscillation wavelength is fixed at 25 nm at 25°C [30]. The OWD technique has been applied to various semiconductor lasers to improve their performance at a high temperature [25,31]. In this study, the influence of this mismatch on the QD lasers is analyzed. A high-reflection (HR) coating with reflectivity of 95% and an antireflection (AR) coating with reflectivity of 3% are applied to the rear and front facets, respectively, to break the longitudinal symmetry and operate at a single longitudinal mode. Due to the interference between the grating and the HR facet, the lasing properties are dependent on cleavage plane variations. In consequence, AR/HR DFB lasers can emit light either at the Bragg wavelength or at another wavelength located within the laser stopband; this design is also able to maximize the output power from the output facet [32]. More detailed device fabrication process information is available elsewhere [33].

Figure 1(a) depicts the light-current (L-I) characteristics of the QD DFB laser operating under different temperatures. The device studied exhibits a strong lasing stability over a wide temperature range, by ensuring a sufficient output power over 15 mW from 15°C to 55°C. The variation of the operation temperature T is found to influence other lasing features

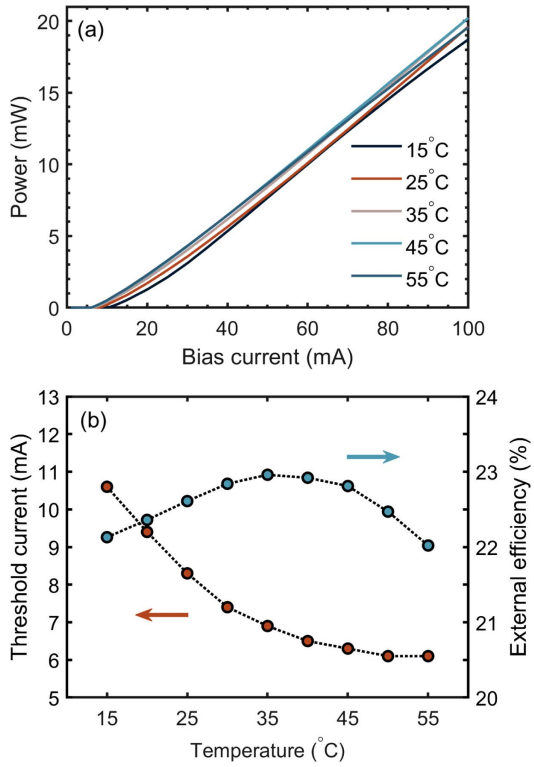

Fig. 1. (a) Light-current characteristics with temperature ranging from 15°C to 55°C. (b) Threshold current (burgundy) and external efficiency (jade) as a function of temperature.

including threshold current I_{th} (burgundy) and external efficiency η (jade) as shown in Fig. 1(b). The latter is calculated through $\eta = \frac{q\lambda}{hc}\frac{\Delta P}{\Delta I}$, with h the Planck constant, c the speed of light, q the electron charge, and λ the lasing wavelength. The threshold current decreases with T down to a few milliamps, meaning that a smaller OWD at a higher temperature is beneficial for reducing the internal loss [28,34,35]. Besides, the benefit brought by a small OWD can also be confirmed by the increase of external efficiency with temperature up to 40°C, and the maximum external efficiency is 23%. Once the temperature increases above 40°C, however, the active region of the laser suffers from a stronger carrier thermalization that leads to more nonradiative recombination, whose presence results in the decrease of the external efficiency as depicted in Fig. 1(b). Nevertheless, it is worth stressing that this inconvenience can be partially compensated by the consecutive reduction of internal loss with the increase of temperature; up to 55°C, we do not observe a reincrease of the threshold current. Moreover, the laser performance can be still improved at a high temperature above 40°C by the OWD technique, which is discussed hereinafter.

Figure 2 depicts the optical spectra of the device at $2 \times I_{\mathrm{th}}$ by increasing the temperature from 15°C to 55°C. The multimode lasing dynamics observed across the gain peak are magnified when decreasing the temperature down to 15°C. This multimode dynamic results from the contribution of the different QD populations that are desynchronized at a low temperature through the temperature-dependent homogeneous gain broadening. In addition, let us stress that the reduction of the gain and the multimode operation also illustrates why the output power decreases at a low temperature. Furthermore, in DFB semiconductor lasers, the temperature-dependent OWD can be described by the following relationship:

$$\lambda_0 - \lambda_p \approx \left(\frac{\mathrm{d}\lambda_0}{\mathrm{d}T} - \frac{\mathrm{d}\lambda_p}{\mathrm{d}T}\right)(T - T_{\mathrm{m}}), \tag{1}$$

where λ_0 and λ_p are the wavelength of the DFB mode and that at the gain peak, respectively, and $\mathrm{d}\lambda_0/\mathrm{d}T$ and $\mathrm{d}\lambda_p/\mathrm{d}T$ are the corresponding temperature coefficients. The temperature

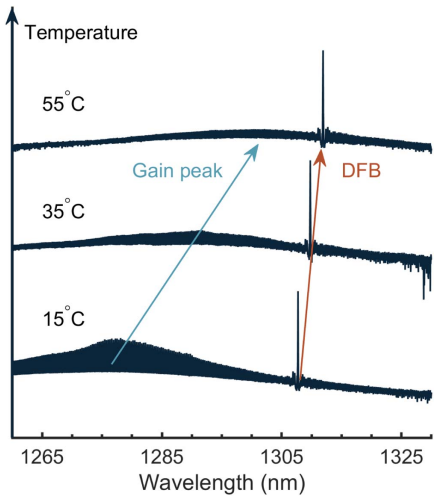

Fig. 2. Optical spectra of the QD DFB laser from 15°C to 55°C ($2 \times I_{\mathrm{th}}$).

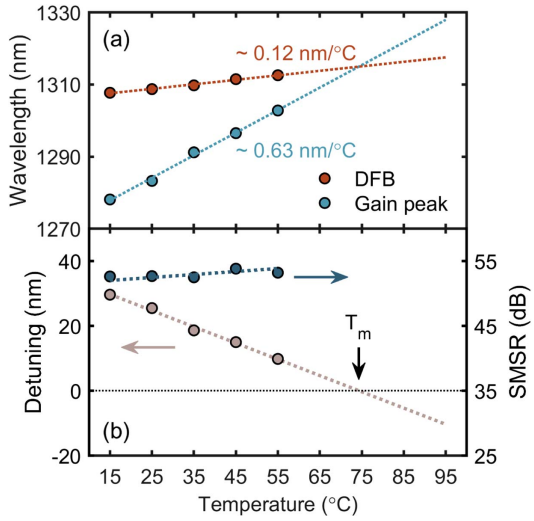

Fig. 3. Temperature-dependent (a) DFB wavelength (burgundy), optical gain peak (jade), (b) optical wavelength detuning (gray), and side-mode suppression ratio (emerald).

where λ_0 is coincident with λ_p is described as T_{m}. In this study, the evolution of the wavelength shift of λ_0 (burgundy) and λ_p (jade) as a function of temperature variation is shown in Fig. 3(a). The lasing wavelength of the DFB laser is determined by the temperature-dependent refractive index of the material composing DFB laser active region, whereas that of the gain peak is determined by the temperature-dependent material gain. In the device studied, the temperature-induced wavelength shift is at 0.12 nm/°C and 0.63 nm/°C for λ_0 and λ_p, respectively. From Eq. (1), it turns out that the optimal performance of a DFB laser occurs at the temperature T_{m}, that is to say, for $\lambda_0 = \lambda_p$ [34]. In this study, the optical detuning vanishes for $T_m \simeq 75$°C, which corresponds to the optimum temperature condition. Figure 3(b) depicts the temperature-dependent OWD (gray), and the side-mode suppression ratio (SMSR, emerald) of the DFB laser. Experimental results also demonstrate that a high SMSR over 50 dB is always maintained over the entire temperature ranging from 15°C to 55°C. These results confirm that an optimum wavelength mismatch is an efficient approach to design a single-frequency source for an uncooled photonic integrated system.

3. RELATIVE INTENSITY NOISE AND MODULATION DYNAMIC PROPERTIES

Optical transceivers with low relative intensity noise (RIN) are required for carrying broadband data with low bit error rate [36]. The RIN properties of the DFB laser studied are therefore investigated in this section. To do so, the output light is coupled into a lens-end fiber, and then it is sent to a low-noise photodiode with a bandwidth of 10 GHz. The AC signal is amplified by a broadband amplifier with a typical small-signal gain of 30 dB, while the DC voltage is measured by a voltage meter through the DC monitor port of the photodiode. The amplified noise spectrum is measured on an electrical spectrum analyzer. More details of the experimental configurations can be found in Ref. [19]. Note that the measured intensity noise

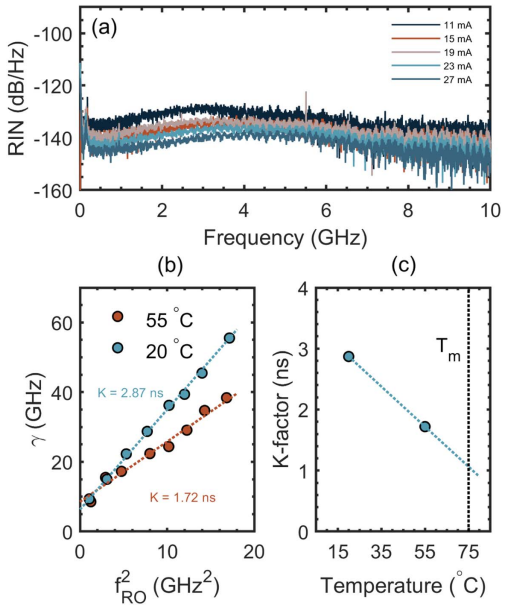

Fig. 4. (a) Measured RIN spectra at several bias currents at 20°C. (b) Extracted damping factor γ as a function of the squared relaxation oscillation frequency f_{RO}^2 at 20°C (jade) and at 55°C (burgundy). (c) Tendency of K-factor versus the temperature; T_{m} is marked by the black dashed line.

spectrum reflects the contribution of the fluctuation in carrier density but not including the shot noise, since the RIN level is usually much higher [37]. Figure 4(a) depicts the RIN spectra in different bias conditions at 20°C, and the bias current ranging from 11 to 27 mA corresponding to each spectrum is marked in the same color. Owing to the low spontaneous emission factor, RIN values as low as −150 to − 160 dB/Hz have been reported in the past few years in both native and silicon-based QD lasers [17,19,38]. In this study, a low RIN level of −150 dB/Hz at 10 GHz is also demonstrated. By increasing the bias current, the peak of the relaxation oscillation frequency (ROF) moves from 1 GHz to about 4 GHz, until the received power attained the maximal limit of the photodiode beyond $3 \times I_{\mathrm{th}}$ (0.72 mW). In what follows, both the ROF and damping factor γ are then extracted independently by curve-fitting the RIN spectrum through the relationship [19,36]

$$\mathrm{RIN}(\omega) = \frac{a + b\omega^2}{(\omega^2 - \omega_{\mathrm{RO}}^2)^2 + \omega^2\gamma^2}, \tag{2}$$

where ω_{RO} is the angular ROF, γ is the damping factor, ω is the angular frequency, and a and b are the coefficients used for the curve fitting.

Figure 4(b) displays the damping factor as a function of the squared ROF at 20°C (jade) and at 55°C (burgundy). The linear evolution is defined as $\gamma = K f_{\mathrm{RO}}^2 + \gamma_0$ with K the K-factor, γ_0 the damping factor offset associated with the inverse of the differential carrier lifetime (τ_c), and f_{RO} the ROF. The K-factor and γ_0 of the device at 20°C are thus measured as 2.9 ns and 6.3 GHz, respectively. As the temperature increases to 55°C, the K-factor decreases to 1.7 ns, whereas γ_0 shifts to 8.5 GHz. Table 1 summarizes the room-temperature device

Table 1. Modulation Dynamic Performance between InAs QD Lasers Grown on GaAs and on Si Substrate at Room Temperature

Reference		[39]	[40]	[41]	[19]
Substrate	GaAs	GaAs	GaAs	Si	Si
I_{th} (mA)	9.3	9.2	14.0	14.0	23.0
L_{cav} (mm)	0.75	0.3-0.4	0.4	0.58	1.35
K (ns)	2.90	0.90	0.68	0.92	1.70
$f_{3\,\mathrm{dB,\,max}}$ (GHz)	3.0	9.9	13.1	9.7	5.2

parameters of this work aggregated with those previously reported in 1.3 μm InAs QD lasers grown on either native GaAs substrate or silicon substrate (with sole ground-state lasing). It is worth stressing that a low K-factor typically below 1 ns is desired to ensure a large maximum 3 dB bandwidth $f_{3\,\mathrm{dB,\,max}} = 2\sqrt{2}\pi/K$ [39,41]. To increase the modulation capabilities, shortening the cavity length below 500 μm is preferred. The modulation bandwidth can also be increased with p-modulation doping of the active region in order to improve the carrier transport across the barrier [41]. In this study, the large K-factor is attributed to the low differential gain at room temperature [42,43]. However, when the OWD is reduced, the K-factor drops down to 1.7 ns at 55°C and can be further reduced in the optimum temperature condition T_{m}. As illustrated in Fig. 4(c), the K-factor is estimated to be below 1 ns at T_{m} where the differential gain is at its maximum value. Note that another important parameter ruling out the K-factor is the gain compression factor ϵ_P [42]. The gain compression is caused by a cascade of complex processes such as carrier heating and spatial and spectral hole burning [22,44,45]. In this study, the determination of the gain compression factor with respect to the output power ϵ_P is performed in Section 4. Its value ranges between 3×10^{-2} and 7×10^{-2} mW^{-1} in the full temperature range (15°C–55°C), meaning that it contributes little to the large K-factor measured. Last but not least, the strong damping together with the low gain compression suggests a high degree of resistance against backreflections as discussed hereinafter.

4. LINEWIDTH ENHANCEMENT FACTOR

The linewidth enhancement factor is known to be a gain-medium parameter to describe the carrier density dependencies of gain and carrier-induced refractive index. A material with near-zero α factor is highly expected to be the active region for semiconductor lasers to improve their resistance to backreflection [46], and the QDs are ideal solutions for on-chip light sources to approach isolator-free applications [22,47]. Several methods have been proposed to measure the α factor of optoelectronics devices such as amplified spontaneous emission (ASE) [48], injection-locking [49], and FM/AM [50]. In this work, the α factor is extracted using the sinusoidal optical phase modulation technique [51], which allows to extract the above-threshold α factor without introducing thermal effects. In the measurements, the device is directly modulated by a sine wave within the small signal modulation regime. The sinusoidal signal is supplied by a radio-frequency (RF) generator at a modulation frequency f_{m} of 12 GHz, which is high enough to

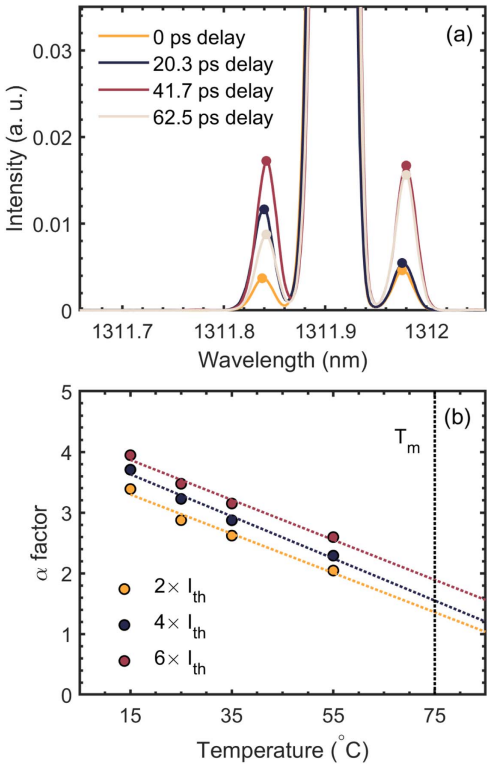

Fig. 5. (a) Optical spectra around the DFB mode and the modulation sidebands of the DFB laser operating at $2 \times I_{th}$ under 55°C. The spectra obtained for four different optical delays are normalized to the main lobes. (b) Effective α factor in different operation conditions. T_m is marked by the black dashed line.

approach $\alpha \simeq 2\beta/m$, where β and m are the frequency modulation index and the amplitude modulation index, respectively [52]. The optical signal is then sent to a fiber coupled phase modulator that is modulated at the same f_m. An optical delay line is placed between the DFB laser and the phase modulator in order to control the delay between the optical and electrical signals at the input of the phase modulator [53]. The output signal from the modulator is finally sent to a high-resolution optical spectrum analyzer to resolve the optical carrier and the modulation sidebands. More details of the experimental configurations can be found in Ref. [51]. Figure 5(a) depicts the optical spectra corresponding to four different delays equally spaced by $1/f_m$ being 20.3 ps, when the DFB laser operates at $2 \times I_{th}$ under 55°C. By increasing the delay length $(k-1)/f_m$ from $k = 1$ to $k = 4$ (k is an integer), the peaks of the left and right side modes normalized to the main lobe are retrieved as I_{-1}^k and I_{+1}^k, respectively. The α factor can therefore be calculated by the following relationship [51]:

$$\alpha = \frac{\mathrm{Im}(\sqrt{Q_{-1}Q_{+1}})}{\mathrm{Re}(\sqrt{Q_{-1}Q_{+1}})}, \tag{3}$$

with

$$\begin{aligned} Q_{-1} &= (I_{-1}^1 - I_{-1}^3) + j(I_{-1}^0 - I_{-1}^2), \\ Q_{+1} &= (-I_{+1}^1 + I_{+1}^3) + j(I_{+1}^0 - I_{+1}^2). \end{aligned} \tag{4}$$

The effective α factors measured in different operation conditions are shown in Fig. 5(b). By increasing the bias current, the enlargement of the α factor in agreement with previous work [20,45] is attributed to the gain compression. In all temperature conditions, the effective α factor exhibits a strong stability against the current variation. As shown, its value enlarges from 2 to 2.6 with the increasing bias current from $2 \times I_{th}$ to $6 \times I_{th}$ at 55°C. These features indicate that the corresponding gain compression coefficients ϵ_P are quite low. Indeed, the ϵ_P can be estimated by the variation of above-threshold α factor as a function of output power P, according to the relationship $\alpha(P) = \alpha_{GS}(1 + \epsilon_P P) + \alpha_{ES}(1 - \epsilon_P P)^{-1}$, where α_{GS} and α_{ES} are the α factor at the threshold of the ground state (GS) and excited state (ES), respectively [45]. In this study, the second term of the aforementioned equation can be omitted since the device studied exhibits sole GS emission. The ϵ_P measured thus slightly changes from 2×10^{-2} to 7×10^{-2} mW^{-1} with the increase of temperature from 15°C to 55°C. These low values are rather found similar to those of QW lasers than those observed on other QD devices [19,45]. On the other hand, our results reveal that the above-threshold α factor exhibits a strong dependence of the operation temperature through the wavelength mismatch. Discussions in Section 3 demonstrate that the reduced OWD decreases the internal loss, thus resulting in the increase of differential gain, and hence the effective α factor minimizes. For instance, the α factor reduces from 3.4 to 2 by increasing the temperature from 15°C to 55°C, when the device operates at $2 \times I_{th}$. It is worth stressing that the α factor can be further minimized once the temperature increases to T_m. These results bring novel insight in designing DFB lasers, given that the detuning between the Bragg wavelength and the optical gain peak can be properly optimized to minimize the α factor at a high temperature. The laser performance such as its tolerance for optical feedback can thus be largely improved. Corresponding discussions are performed in Section 5.

5. NONLINEAR DYNAMICS

In this section, we investigate the nonlinear dynamics of the DFB laser in presence of coherent EOF. The EOF process involved in a semiconductor laser is described as the amplitude-phase coupling in the active region between the feedback light field and that of the intra-cavity, which results in the field fluctuation both in amplitude and phase [20]. The returned field that is coupled back to the laser cavity brings both a phase fluctuation and a perturbation on the photon density, and the latter leads to a fluctuation of the carrier density and the optical gain. The gain variation therefore impacts the refractive index through the α factor, hence resulting in a deviation of the lasing wavelength. It is worth stressing that the phase fluctuation induced from the returned field is also associated with the wavelength fluctuation; however, its impact is minimized in the long-cavity feedback regime where the external cavity length exceeds the coherence length [9,23]. Therefore, the laser system can suffer from severe optical instabilities such as coherence collapse (CC) operation in the presence of EOF. To characterize the coherent reflection sensitivity, an approach to estimate the critical feedback level r_{crit} for CC operation is described as follows [36]:

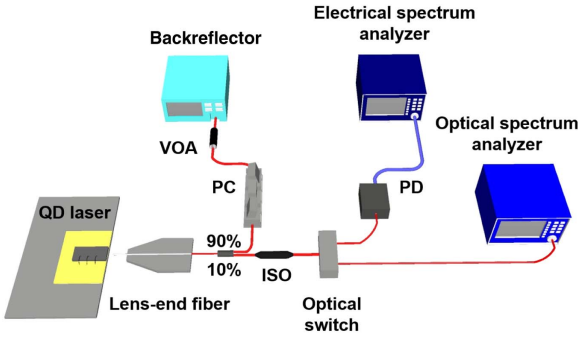

Fig. 6. Experimental setup used for the long-delay coherent external optical feedback measurement. ISO, optical isolator; PD, photodiode; PC, polarization controller; VOA, variable optical attenuator.

$$r_{\mathrm{crit}} = \frac{\tau_L^2 \gamma^2}{16C^2}\left(\frac{1+\alpha^2}{\alpha^4}\right), \tag{5}$$

where τ_L is the photon cavity round-trip time, and C is the cavity coupling factor depending on the grating parameters, the facet reflectivities, and phases for the case of DFB lasers [54,55]. By following Eq. (5), the QDs, being the gain medium of semiconductor lasers, exhibit a strong potential for improving their feedback resistance, owing to the stronger damping and possibly the smaller α factor over QWs [22]. In this study, the diminution of the α factor with the increase of temperature suggests an improved immunity against the parasitic reflections [56].

Figure 6 schematically depicts the experimental configurations for EOF. Laser emission is coupled by an AR-coated lens-end fiber, and 90% of the coupled power is sent to the 12 m long-delay feedback path, where the light is reflected back to the laser cavity. In the experiments, such a 12 m long external cavity ensures that the ROF of the laser is well beyond the external cavity frequency, and hence the impact of the phase is negligible. The backreflector combined with a variable optical attenuator (VOA) is then wired to change the feedback strength r_{ext}. In this work, r_{ext} is defined as the ratio between the power returned to the laser cavity and the free-space emitting power of the laser, and the practical achievable r_{ext} ranges from 0% to 30%. A polarization controller is inserted in the external cavity to compensate for the polarization rotation in the fiber, which hence maximizes the effects of EOF. The remaining 10% of coupled light is transferred to an optical switch, where the signal can be swapped between the optical and electrical spectrum analyzer for further analysis.

Figure 7 displays the feedback dynamics both in the RF and optical domains and for two different bias conditions, when the DFB laser operates at 25°C where the OWD remains large. The first column depicts the behaviors at $2 \times I_{\mathrm{th}}$, and the second column depicts those at $6 \times I_{\mathrm{th}}$. The first and second rows present the RF spectra and the RF power mapping, whereas the third and fourth rows correspond to the optical spectra and the spectral power mapping. Operating at $2 \times I_{\mathrm{th}}$, the device studied remains stable against EOF up to $r_{\mathrm{crit}} = 2.5\%$, and then it directly enters into CC operation regime. First, the periodic oscillation [gold spectrum in Fig. 7(a)] induced

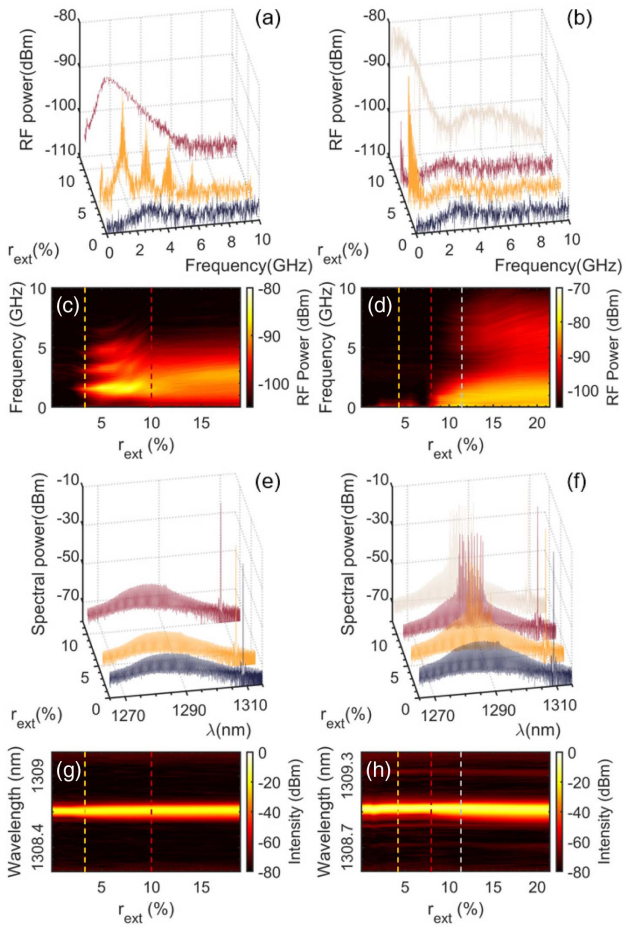

Fig. 7. RF spectra and optical spectra in different r_{ext} conditions, when the DFB laser operates at [(a) and (e)] $2 \times I_{\mathrm{th}}$ and [(b) and (f)] $6 \times I_{\mathrm{th}}$ at 25°C. Corresponding power mapping of the RF and optical spectra as a function of r_{ext} [(c) and (g)] at $2 \times I_{\mathrm{th}}$ and [(d) and (h)] at $6 \times I_{\mathrm{th}}$.

by the undamped relaxation oscillation takes place at the onset of the instabilities, and the ROF together with its higher harmonics is identified; then the CC operation is fully developed with a stronger r_{ext}, and the laser exhibits chaotic oscillation [burgundy spectrum in Fig. 7(a)]. Corresponding r_{ext} to these spectra are marked by the gold and burgundy dashed lines in Fig. 7(c), respectively. In such a low bias condition, the DFB laser remains single-mode oscillation except for the mode broadening in the regime of CC operation as shown in Figs. 7(e) and 7(g).

More regimes on the route to CC are identified when the bias current increases to $6 \times I_{\mathrm{th}}$. In this study, four regimes are retrieved in agreement with a prior study [9]. All the r_{ext} corresponding to the spectra in Figs. 7(b) and 7(f) are remarked by the dashed lines in the same colors in Figs. 7(d) and 7(h). In regime I where the r_{ext} is below 2%, the DFB laser remains stable. With an r_{ext} ranging from 2% to 6%, the laser enters into regime II where the dual-wavelength lasing takes place and a series of low-frequency peaks are observed in the RF response [gold spectra in Figs. 7(b) and 7(d)]. Different from the mode hopping observed in a prior study [9], the DFB mode in this

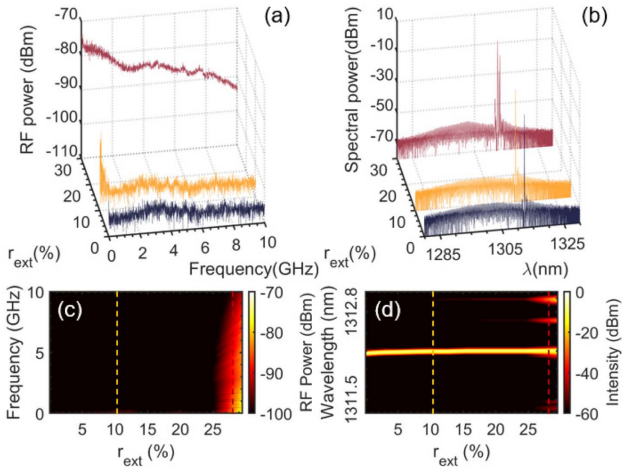

Fig. 8. (a), (b) RF spectra and optical spectra in different r_{ext} conditions, when the DFB laser operates at $6 \times I_{th}$ at 55°C. (c), (d) Corresponding power mapping of the RF and optical spectra as a function of r_{ext}.

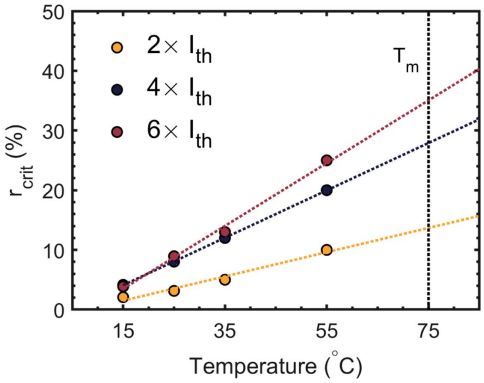

Fig. 9. Critical feedback level r_{crit} associated with the onset of coherence collapse (CC) operation under different operation conditions. T_m is marked by the black dashed line.

study suffers from a wavelength fluctuation within the transition from regime I to regime II. However, the observed peaks induced by the external cavity modes are different from the low-frequency fluctuations that take place in the long-cavity regime [57,58]. By increasing the r_{ext} to ~7%, the low-frequency peaks are largely suppressed, which means the device restabilizes and enters into regime III [burgundy spectrum in Fig. 7(b)]. Nevertheless, this operation regime is too narrow to observe the restabilization in the optical spectrum [burgundy spectrum in Fig. 7(f)]. Further increasing the r_{ext} above 8%, which is defined as the r_{crit} in this study, the laser enters into regime IV in the presence of the DFB mode broadening and chaotic oscillations [gray spectra in Figs. 7(b) and 7(f)]. In such a high bias condition, the DFB laser is overdamped, and it does not show any periodic oscillation in regime IV.

In aforementioned sections, discussions reveal that a near-zero OWD that occurs at a high temperature is beneficial for improving laser performances, especially the decrease of the effective α factor. According to Eq. (5), the feedback insensitivity of device can thus be largely enhanced. Figure 8 displays the feedback dynamics at $6 \times I_{th}$ both in the RF and optical domains, when the device studied operates near the optimum temperature condition at 55°C. Corresponding r_{ext} to the performed spectra are marked by the gold and burgundy dashed lines in Figs. 8(c) and 8(d). In this case, the onset of regime II occurs at r_{ext} being 5%, where the external cavity frequencies are observed [gold spectrum in Fig. 8(a)]; however, different from the phenomena observed at 25°C, the optical spectrum remains stable without showing either multimode lasing on the gain peak or DFB mode broadening [gold spectrum in Fig. 8(b)]. Thus, a small OWD is also beneficial for reducing the strength of the external cavity frequencies in regime II. By increasing the r_{ext} up to ~25%, regime III is too narrow to be observed, and the laser directly enters into regime IV by performing CC operation both in the RF and optical domains [burgundy spectra in Figs. 8(a) and 8(b)], where both the broadening of the DFB mode and the lasing of the side modes are observed.

Figure 9 depicts the r_{crit} as a function of temperature in different bias conditions. Results demonstrate that the feedback resistance of the device studied is largely improved by reducing the OWD, which is confirmed by the increase of r_{crit} from 4% (−14 dB) to 25% (−6 dB) at $6 \times I_{th}$. The tolerance for feedback can be further improved at T_m as displayed from the different tendency lines. On the other hand, in all temperature conditions, r_{crit} increases with the bias current until $4 \times I_{th}$ at which saturation is observed. This behavior in agreement with prior studies [59,60] is attributed to the enlarged intra-cavity photon density with the bias current, whereas the saturation of r_{crit} at a high bias results from the overdamping of the laser.

6. CONCLUSIONS

In this paper, we report an in-depth investigation on a 1.3 μm InAs/GaAs QD single-frequency laser specifically designed to increase the maximum lasing temperature. The effect of the optical mismatch between the optical gain peak and the oscillation wavelength is studied and linked to the static, dynamic, and nonlinear characteristics of the QD laser. In particular, we show that the combination of QDs as a gain medium and an optical wavelength detuning as large as 25 nm at room temperature allows us to successfully fully control the thermal effects. In this context, the increase of operation temperature is no longer a limiting factor of the device performance. With the design of an optimum temperature condition of 75°C, this DFB laser enables the best performance at a high temperature in terms of threshold current, output power, α factor, intensity noise, modulation dynamics, and reflection insensitivity. Importantly, the OWD technique is able to be applied to various semiconductor lasers to enhance their performance at a high temperature. Nevertheless, the QDs with a high degree of thermal stability maximize the improvement of performance. To sum up, the large optical mismatch assisted single-frequency QD DFB laser exhibits a strong potential not only for isolator-free applications but also for emerging markets that require high-temperature operations and improved coherent light

sources, such as resource findings in deep underground, mobile applications, and uncooled integrated systems.

Funding. Advanced Research Projects Agency—Energy (DE-AR0001039).

Acknowledgment. The authors acknowledge the financial support of the Institut Mines-Télécom.

Disclosures. The authors declare no conflicts of interest.

Data Availability. No data were generated or analyzed in the presented research.

REFERENCES

1. R. Jones, P. Doussiere, J. B. Driscoll, W. Lin, H. Yu, Y. Akulova, T. Komljenovic, and J. E. Bowers, "Heterogeneously integrated InP/silicon photonics: fabricating fully functional transceivers," IEEE Nanotechnol. Mag. **13**, 17–26 (2019).
2. K. Numata, J. R. Chen, S. T. Wu, J. B. Abshire, and M. A. Krainak, "Frequency stabilization of distributed-feedback laser diodes at 1572 nm for lidar measurements of atmospheric carbon dioxide," Appl. Opt. **50**, 1047–1056 (2011).
3. S. Matsuo, T. Fujii, K. Hasebe, K. Takeda, T. Sato, and T. Kakitsuka, "Directly modulated DFB laser on SiO_2/Si substrate for datacenter networks," J. Lightwave Technol. **33**, 1217–1222 (2015).
4. J. Duan, H. Huang, Z. Lu, P. Poole, C. Wang, and F. Grillot, "Narrow spectral linewidth in InAs/InP quantum dot distributed feedback lasers," Appl. Phys. Lett. **112**, 121102 (2018).
5. N. Andriolli, F. Bontempi, and G. Contestabile, "InP monolithically integrated transmitters based on high speed directly modulated DFB lasers," IEEE J. Sel. Top. Quantum Electron. **26**, 1500606 (2020).
6. H. Nishimoto, M. Yamaguchi, I. Mito, and K. Kobayashi, "High-frequency response for DFB LD due to a wavelength detuning effect," J. Lightwave Technol. **5**, 1399–1402 (1987).
7. H. Cantú, A. McKee, D. Childs, S. Watson, and A. Kelly, "Dynamic performance of detuned ridge waveguide AlInGaAs distributed feedback laser diodes," Microw. Opt. Technol. Lett. **59**, 1468–1470 (2017).
8. K. Schires, N. Girard, G. Baili, G.-H. Duan, S. Gomez, and F. Grillot, "Dynamics of hybrid III-V silicon semiconductor lasers for integrated photonics," IEEE J. Sel. Top. Quantum Electron. **22**, 43–49 (2016).
9. R. Tkach and A. Chraplyvy, "Regimes of feedback effects in 1.5-μm distributed feedback lasers," J. Lightwave Technol. **4**, 1655–1661 (1986).
10. J. Mørk, J. Mark, and B. Tromborg, "Route to chaos and competition between relaxation oscillations for a semiconductor laser with optical feedback," Phys. Rev. Lett. **65**, 1999–2002 (1990).
11. K. Petermann, "External optical feedback phenomena in semiconductor lasers," IEEE J. Sel. Top. Quantum Electron. **1**, 480–489 (1995).
12. D. Lenstra, B. Verbeek, and A. Den Boef, "Coherence collapse in single-mode semiconductor lasers due to optical feedback," IEEE J. Quantum Electron. **21**, 674–679 (1985).
13. H. Huang, J. Duan, D. Jung, A. Y. Liu, Z. Zhang, J. Norman, J. E. Bowers, and F. Grillot, "Analysis of the optical feedback dynamics in InAs/GaAs quantum dot lasers directly grown on silicon," J. Opt. Soc. Am. B **35**, 2780–2787 (2018).
14. D. Lenstra, T. T. M. van Schaijk, and K. A. Williams, "Toward a feedback-insensitive semiconductor laser," IEEE J. Sel. Top. Quantum Electron. **25**, 1502113 (2019).
15. F. Klopf, J. Reithmaier, and A. Forchel, "Highly efficient GaInAs/(Al)GaAs quantum-dot lasers based on a single active layer versus 980 nm high-power quantum-well lasers," Appl. Phys. Lett. **77**, 1419–1421 (2000).
16. A. Ukhanov, A. Stintz, P. Eliseev, and K. Malloy, "Comparison of the carrier induced refractive index, gain, and linewidth enhancement factor in quantum dot and quantum well lasers," Appl. Phys. Lett. **84**, 1058–1060 (2004).
17. A. Capua, L. Rozenfeld, V. Mikhelashvili, G. Eisenstein, M. Kuntz, M. Laemmlin, and D. Bimberg, "Direct correlation between a highly damped modulation response and ultra low relative intensity noise in an InAs/GaAs quantum dot laser," Opt. Express **15**, 5388–5393 (2007).
18. Z. Lu, J. Liu, C. Song, J. Weber, Y. Mao, S. Chang, H. Ding, P. Poole, P. Barrios, D. Poitras, S. Janz, and M. O'Sullivan, "High performance InAs/InP quantum dot 34.462-GHz C-band coherent comb laser module," Opt. Express **26**, 2160–2167 (2018).
19. J. Duan, Y. Zhou, B. Dong, H. Huang, J. C. Norman, D. Jung, Z. Zhang, C. Wang, J. E. Bowers, and F. Grillot, "Effect of p-doping on the intensity noise of epitaxial quantum dot lasers on silicon," Opt. Lett. **45**, 4887–4890 (2020).
20. H. Huang, J. Duan, B. Dong, J. Norman, D. Jung, J. E. Bowers, and F. Grillot, "Epitaxial quantum dot lasers on silicon with high thermal stability and strong resistance to optical feedback," APL Photon. **5**, 016103 (2020).
21. M. Matsuda, N. Yasuoka, K. Nishi, K. Takemasa, T. Yamamoto, M. Sugawara, and Y. Arakawa, "Low-noise characteristics on 1.3-μm-Wavelength quantum-dot DFB lasers under external optical feedback," in *IEEE International Semiconductor Laser Conference (ISLC)* (IEEE, 2018), pp. 1–2.
22. J. Duan, H. Huang, B. Dong, J. C. Norman, Z. Zhang, J. E. Bowers, and F. Grillot, "Dynamic and nonlinear properties of epitaxial quantum dot lasers on silicon for isolator-free integration," Photon. Res. **7**, 1222–1228 (2019).
23. B. Dong, J.-D. Chen, F.-Y. Lin, J. C. Norman, J. E. Bowers, and F. Grillot, "Dynamic and nonlinear properties of epitaxial quantum-dot lasers on silicon operating under long-and short-cavity feedback conditions for photonic integrated circuits," Phys. Rev. A **103**, 033509 (2021).
24. A. Y. Liu, S. Srinivasan, J. Norman, A. C. Gossard, and J. E. Bowers, "Quantum dot lasers for silicon photonics," Photon. Res. **3**, B1–B9 (2015).
25. T. Katsuyama, "Development of semiconductor laser for optical communication," SEI Tech. Rev. **69**, 13–20 (2009).
26. G. P. Agrawal and N. K. Dutta, *Semiconductor Lasers* (Kluwer Academic, 2013).
27. G. Morthier and P. Vankwikelberge, *Handbook of Distributed Feedback Laser Diodes* (Artech House, 2013).
28. K. Nishi, K. Takemasa, M. Sugawara, and Y. Arakawa, "Development of quantum dot lasers for data-com and silicon photonics applications," IEEE J. Sel. Top. Quantum Electron. **23**, 1901007 (2017).
29. H. Soda, Y. Kotaki, H. Sudo, H. Ishikawa, S. Yamakoshi, and H. Imai, "Stability in single longitudinal mode operation in GaInAsP/InP phase-adjusted DFB lasers," IEEE J. Quantum Electron. **23**, 804–814 (1987).
30. K. Takada, Y. Tanaka, T. Matsumoto, M. Ekawa, H. Song, Y. Nakata, M. Yamaguchi, K. Nishi, T. Yamamoto, M. Sugawara, and Y. Arakawa, "Wide-temperature-range 10.3 Gbit/s operations of 1.3 μm high-density quantum-dot DFB lasers," Electron. Lett. **47**, 206–208 (2011).
31. S. J. Jeong, J. K. Kang, K. Oh, B. K. Kang, T.-J. Kim, and Y. Sin, "Effect of wavelength detuning on spectral and temperature characteristics of 1.3-μm DFB lasers," Proc. SPIE **3001**, 394–399 (1997).
32. C. Henry, "Performance of distributed feedback lasers designed to favor the energy gap mode," IEEE J. Quantum Electron. **21**, 1913–1918 (1985).
33. K. Nishi, T. Kageyama, M. Yamaguchi, Y. Maeda, K. Takemasa, T. Yamamoto, M. Sugawara, and Y. Arakawa, "Molecular beam epitaxial growths of high-optical-gain InAs quantum dots on GaAs for long-wavelength emission," J. Cryst. Growth **378**, 459–462 (2013).
34. H. Lu, C. Blaauw, and T. Makino, "Single-mode operation over a wide temperature range in 1.3 μm InGaAsP/InP distributed feedback lasers," J. Lightwave Technol. **14**, 851–859 (1996).
35. K. Takada, Y. Tanaka, T. Matsumoto, M. Ekawa, Y. Nakata, T. Yamamoto, M. Sugawara, and Y. Arakawa, "Temperature-stable 10.3-Gb/s operation of 1.3-μm quantum-dot DFB lasers with GaInP/GaAs gratings," in *National Fiber Optic Engineers Conference* (Optical Society of America, 2009), paper JWA28.
36. L. A. Coldren, S. W. Corzine, and M. L. Mashanovitch, *Diode Lasers and Photonic Integrated Circuits* (Wiley, 2012), Vol. **218**.

37. Y.-G. Zhou, C. Zhou, C.-F. Cao, J.-B. Du, Q. Gong, and C. Wang, "Relative intensity noise of InAs quantum dot lasers epitaxially grown on Ge," Opt. Express **25**, 28817–28824 (2017).
38. F. Lelarge, B. Dagens, J. Renaudier, R. Brenot, A. Accard, F. van Dijk, D. Make, O. Le Gouezigou, J.-G. Provost, F. Poingt, J. Landreau, O. Drisse, E. Derouin, B. Rousseau, F. Pommereau, and G.-H. Duan, "Recent advances on InAs/InP quantum dash based semiconductor lasers and optical amplifiers operating at 1.55 μm," IEEE J. Sel. Top. Quantum Electron. **13**, 111–124 (2007).
39. D. Arsenijević and D. Bimberg, "Quantum-dot lasers for 35 Gbit/s pulse-amplitude modulation and 160 Gbit/s differential quadrature phase-shift keying," Proc. SPIE **9892**, 98920S (2016).
40. Y. He, Z. Zhang, Z. Lv, T. Yang, D. Lu, and L. Zhao, "10-Gbps 20-km feedback-resistant transmission using directly modulated quantum-dot lasers," IEEE Photon. Technol. Lett. **32**, 1353–1356 (2020).
41. D. Inoue, D. Jung, J. Norman, Y. Wan, N. Nishiyama, S. Arai, A. C. Gossard, and J. E. Bowers, "Directly modulated 1.3 μm quantum dot lasers epitaxially grown on silicon," Opt. Express **26**, 7022–7033 (2018).
42. A. Fiore and A. Markus, "Differential gain and gain compression in quantum-dot lasers," IEEE J. Quantum Electron. **43**, 287–294 (2007).
43. C. Hantschmann, P. P. Vasil'ev, A. Wonfor, S. Chen, M. Liao, A. J. Seeds, H. Liu, R. V. Penty, and I. H. White, "Understanding the bandwidth limitations in monolithic 1.3 μm InAs/GaAs quantum dot lasers on silicon," J. Lightwave Technol. **37**, 949–955 (2018).
44. A. Martinez, Y. Li, L. F. Lester, and A. L. Gray, "Microwave frequency characterization of undoped and p-doped quantum dot lasers," Appl. Phys. Lett. **90**, 251101 (2007).
45. F. Grillot, B. Dagens, J.-G. Provost, H. Su, and L. F. Lester, "Gain compression and above-threshold linewidth enhancement factor in 1.3-μm InAs-GaAs quantum-dot lasers," IEEE J. Quantum Electron. **44**, 946–951 (2008).
46. W. W. Chow, Z. Zhang, J. C. Norman, S. Liu, and J. E. Bowers, "On quantum-dot lasing at gain peak with linewidth enhancement factor $\alpha_H = 0$," APL Photon. **5**, 026101 (2020).
47. Z. Zhang, D. Jung, J. C. Norman, W. W. Chow, and J. E. Bowers, "Linewidth enhancement factor in InAs/GaAs quantum dot lasers and its implication in isolator-free and narrow linewidth applications," IEEE J. Sel. Top. Quantum Electron. **25**, 1900509 (2019).
48. M. Osinski and J. Buus, "Linewidth broadening factor in semiconductor lasers–an overview," IEEE J. Quantum Electron. **23**, 9–29 (1987).
49. G. Liu, X. Jin, and S.-L. Chuang, "Measurement of linewidth enhancement factor of semiconductor lasers using an injection-locking technique," IEEE Photon. Technol. Lett. **13**, 430–432 (2001).
50. J.-G. Provost and F. Grillot, "Measuring the chirp and the linewidth enhancement factor of optoelectronic devices with a Mach–Zehnder interferometer," IEEE Photon. J. **3**, 476–488 (2011).
51. J.-G. Provost, A. Martinez, A. Shen, and A. Ramdane, "Single step measurement of optical transmitters Henry factor using sinusoidal optical phase modulations," Opt. Express **19**, 21396–21403 (2011).
52. R. Schimpe, J. Bowers, and T. L. Koch, "Characterisation of frequency response of 1.5 μm InGaAsP DFB laser diode and InGaAs PIN photodiode by heterodyne measurement technique," Electron. Lett. **22**, 453–454 (1986).
53. I. Kang and C. Dorrer, "Method of optical pulse characterization using sinusoidal optical phase modulations," Opt. Lett. **32**, 2538–2540 (2007).
54. F. Favre, "Theoretical analysis of external optical feedback on DFB semiconductor lasers," IEEE J. Quantum Electron. **23**, 81–88 (1987).
55. F. Grillot, "On the effects of an antireflection coating impairment on the sensitivity to optical feedback of AR/HR semiconductor DFB lasers," IEEE J. Quantum Electron. **45**, 720–729 (2009).
56. B. Dong, J. Duan, C. Shang, H. Huang, A. B. Sawadogo, D. Jung, Y. Wan, J. E. Bowers, and F. Grillot, "Influence of the polarization anisotropy on the linewidth enhancement factor and reflection sensitivity of 1.55-μm InP-based InAs quantum dash lasers," Appl. Phys. Lett. **115**, 091101 (2019).
57. J. Mørk, B. Tromborg, and P. L. Christiansen, "Bistability and low-frequency fluctuations in semiconductor lasers with optical feedback: a theoretical analysis," IEEE J. Quantum Electron. **24**, 123–133 (1988).
58. Y. Takiguchi, H. Fujino, and J. Ohtsubo, "Experimental synchronization of chaotic oscillations in externally injected semiconductor lasers in a low-frequency fluctuation regime," Opt. Lett. **24**, 1570–1572 (1999).
59. S. Azouigui, B. Dagens, F. Lelarge, J. Provost, A. Accard, F. Grillot, A. Martinez, Q. Zou, and A. Ramdane, "Tolerance to optical feedback of 10-Gb/s quantum-dash-based lasers emitting at 1.51 μm," IEEE Photon. Technol. Lett. **19**, 1181–1183 (2007).
60. S. Azouigui, B. Dagens, F. Lelarge, J.-G. Provost, D. Make, O. Le Gouezigou, A. Accard, A. Martinez, K. Merghem, F. Grillot, O. Dehaese, R. Piron, S. Loualiche, Q. Zou, and A. Ramdane, "Optical feedback tolerance of quantum-dot-and quantum-dash-based semiconductor lasers operating at 1.55 μm," IEEE J. Sel. Top. Quantum Electron. **15**, 764–773 (2009).